INTERNATIONAL JOURNAL FOR NUMERICAL METHODS IN FLUIDS, VOL. 6, 35–45 (1986)

AN IMPROVED VORTICITY–POTENTIAL METHOD FOR THREE-DIMENSIONAL DUCT FLOW SIMULATIONS

HERONG YANG AND RICARDO CAMARERO

Ecole Polytechnique de Montreal, Montreal, Canada

SUMMARY

An improved Vorticity–Potential method is presented for the numerical solutions of three-dimensional duct flow problems. The solution procedure requires first a potential solution. Then the viscous effects are added through the vorticity transport equation. By using body-fitted coordinates, the method is applied to simulate the incompressible laminar flows in a square elbow and in a twisted square elbow.

KEY WORDS Vorticity–Potential 3-D Body-Fitted Grid Navier–Stokes Internal Flow

INTRODUCTION

In recent years, a number of numerical approaches have been developed in order to simulate three-dimensional duct flows. Many of them are based on the Vorticity–Potential formulations, which can be regarded as the generalization of the two-dimensional Vorticity–Stream function formulation. Although the stream function has been successfully used in 2-d flow modelling, there has been much confusion over the determination of boundary conditions appropriate to the vector potential. Its applications, therefore, are very limited.

In 1968, Hirasaki and Hellums[1] formally derived the first set of boundary conditions on the vector potential by requiring the solution of a second partial differential equation. Their formulation was relatively simple for confined flows, but too complex for flow-through situations. Later, Hirasaki and Hellums[2] simplified their conditions by introducing a scalar potential. For the flow-through problems, they proposed that the normal derivatives of the scalar potential be the normal components of the velocities on the boundaries. However, this would not be applicable if the specified inlet velocities were rotational, which we will discuss later, or if the outlet velocities were not known *a priori*. Recently, Wong and Reizes[3] demonstrated that it is possible to remove the requirements of the scalar potential by setting an initial velocity component. This is simply the normal component of the specified inlet velocity and maintains the same value along the main flow direction. This technique does reduce somewhat the computational efforts, but its application is restricted to flows in straight ducts of constant cross section. Furthermore, it is not applicable to flows with rotational velocities on the inlet plane.

The purpose of the present paper is to discuss some of the difficulties associated with the boundary conditions on the scalar potential, and present a new set of boundary conditions for the Vorticity–Potential formulations. An improved Vorticity–Potential method is then obtained and shown to be applicable to much more general duct flow situations than the prior techniques.

0271–2091/86/010035–11$01.10

Received 20 February 1985
Revised 20 August 1985

THE VORTICITY–POTENTIAL FORMULATION

The Vorticity–Potential formulation is based on potential theory, which has been fully discussed by Hirasaki and Hellums.[1] For a given velocity field **V**, there exists a vector potential **A** satisfying

$$\mathbf{V} = \nabla \times \mathbf{A}, \tag{1}$$

$$\nabla \cdot \mathbf{A} = 0. \tag{2}$$

The relation between the vector potential **A** and the vorticity **W** is established by taking the curl of equation (1) which yields

$$\nabla^2 \mathbf{A} = -\mathbf{W}, \tag{3}$$

where the vorticity is defined by

$$\mathbf{W} = \nabla \times \mathbf{V}. \tag{4}$$

The boundary conditions on **A**, derived by Hirasaki and Hellums,[1] are

$$\begin{aligned} A_{t_1} &= (\nabla_s \times \mathbf{B})_{t_1}, \\ A_{t_2} &= (\nabla_s \times \mathbf{B})_{t_2}, \\ \nabla \cdot \mathbf{A} &= 0, \end{aligned} \tag{5}$$

where subscripts t_1 and t_2 denote the two tangential components, respectively. The solenoidal condition is applied to determine the normal component, A_n. $\nabla_s \times$ is the surface curl defined as the usual curl with the assumption of

$$\frac{\partial}{\partial n} = 0. \tag{6}$$

B is a vector function defined on the boundary surface. It satisfies the equations

$$\begin{aligned} B_{t_1} &= 0, \\ B_{t_2} &= 0, \\ \mathbf{n} \cdot (\nabla_s \times (\nabla_s \times \mathbf{B})) &= \mathbf{n} \cdot \mathbf{V}. \end{aligned} \tag{7}$$

The main difficulty which arises when using these conditions is to solve for the vector **B**. However, if the velocity vector **V** is aligned with the boundaries, the vector **B** could be set as the null vector. This has been proved by Hirasaki and Hellums.[2] They introduced a scalar potential ϕ through

$$\mathbf{V} = -\nabla\phi + \nabla \times \mathbf{A} \tag{8}$$

with the boundary condition as

$$\frac{\partial \phi}{\partial n} = -\mathbf{n} \cdot \mathbf{V}. \tag{9}$$

Using this technique, **A** is the vector potential of the vector field $\mathbf{V} + \nabla\phi$, which is tangent to all the boundaries. Consequently the boundary conditions on **A** are as follows:

$$\begin{aligned} A_{t_1} &= 0, \\ A_{t_2} &= 0, \\ \frac{\partial A_n}{\partial n} &= 0. \end{aligned} \tag{10}$$

This scalar and vector potential formulation provides an effective means of solving 3-d flow problems, in particular, incompressible flow problems in which the scalar potential ϕ can be solved independently by the equation of continuity

$$\nabla^2\phi = 0. \tag{11}$$

However, as mentioned by Wong and Reizes,[3] one well-known disadvantage is the increased number of equations to be handled. In order to reduce the calculation efforts, Wong and Reizes[3] used a new irrotational component $\mathbf{V}'$ of the velocity $\mathbf{V}$ in place of $-\nabla\phi$:

$$\mathbf{V} = \mathbf{V}' + \nabla \times \mathbf{A}, \tag{12}$$

where $\mathbf{V}'$ is defined as

$$\begin{aligned} \mathbf{V}' &= (\mathbf{n}\cdot\mathbf{V})\mathbf{n}, \quad \text{on the inlet plane,} \\ \mathbf{V}' &= \mathbf{V}'|_{z=z_0} \quad \text{on other sections,} \end{aligned} \tag{13}$$

where z is the coordinate along the flow direction and z_0 is the location of the inlet plane.

It is obvious that this technique eliminates the need to solve for ϕ, but it is restricted to flows in a straight duct of constant cross section. Also it requires the specified inlet velocity to be uniform, otherwise the component $\mathbf{V}'$ is not irrotational. Consequently, this method is not applicable if the flow region has an arbitrary shape, or if the flow has a non-uniform inlet velocity profile.

Another serious problem in the use of scalar and vector potential formulation is associated with the numerical calculation of ϕ. For most duct flow situations, the specified inlet velocity is rotational, as for instance, the flow in a straight duct with a parabolic inlet velocity profile. In those situations, since $\nabla\phi$ is irrotational, it would be extremely difficult for the vector $\nabla\phi$ to fit the boundary conditions of a rotational property.To illustrate this problem, consider a flow situation as shown in Figure 1. Let ϕ_j and $\mathbf{V}_j$ be the values of the scalar potential and the velocity at the nodes P_j. Applying the difference technique to equation (9), we have

$$\begin{aligned} &\phi_1 = \phi_2, && \text{by } V_{1_y} = 0, \\ &\phi_3 = \phi_4, && \text{by } V_{3_y} = 0, \\ &\phi_4 < \phi_2, && \text{by } V_{2_x} > 0, \\ &\phi_1 = \phi_3, && \text{by } V_{1_x} = 0. \end{aligned} \tag{14}$$

It is clear that there is no solution for ϕ at these nodes. Probably this is the reason why Aregbesola and Burley[4] encountered a slow convergence solution of ϕ by assuming a fully developed velocity profile on the exit plane, which is not irrotational.

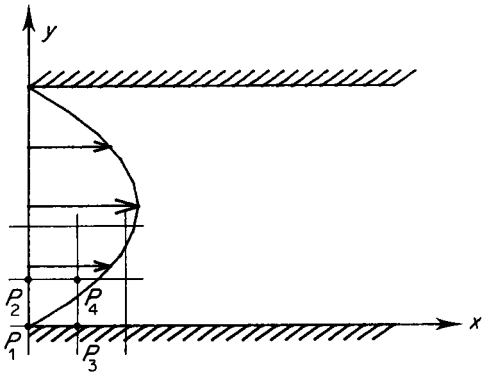

Figure 1. Illustration of inlet velocity profile with rotational property

A NEW SET OF BOUNDARY CONDITIONS

In order to reduce the degree of difficulty in the calculation of ϕ, a new set of boundary conditions is proposed for incompressible flows in ducts of arbitrary cross sections.

Boundary conditions on ϕ

The scalar potential defined by equation (8) is required to satisfy

$$\begin{aligned} \frac{\partial \phi}{\partial n} &= 0 \qquad \text{on solid walls,} \\ \frac{\partial \phi}{\partial n} &= -v_i \qquad \text{on the inlet plane,} \\ \frac{\partial \phi}{\partial n} &= -v_o \qquad \text{on the outlet plane,} \end{aligned} \tag{15}$$

where v_i and v_o are mean velocity values defined by

$$\begin{aligned} v_i &= \iint_{\text{inlet}} \mathbf{n}\cdot\mathbf{V}\,ds, \\ v_o &= v_i(\text{inlet area/outlet area}). \end{aligned} \tag{16}$$

It is obvious that these conditions provide a uniform gradient of ϕ on both inlet and outlet planes, which would be irrotational provided the upstream and downstream tangents are sufficiently long. It is also believed that this technique will accelerate the convergence in solving ϕ, and will result in a higher accuracy.

Boundary conditions on **A**

Applying Hirasaki and Hellums' theory[1] to the vector field $(\mathbf{V} + \nabla\phi)$, we obtain the same boundary conditions on **A** as described by equation (5), but instead of equation (7), **B** satisfies

$$\begin{aligned} B_{t_1} &= 0, \\ B_{t_2} &= 0, \\ \mathbf{n}\cdot(\nabla_s \times (\nabla_s \times \mathbf{B}) &= \mathbf{n}\cdot(\mathbf{V} + \nabla\phi). \end{aligned} \tag{17}$$

For duct flows, these conditions can be simplified as follows.

On the solid walls, the no-slip boundary condition applies:

$$\mathbf{V} = 0.$$

Substituting this and equation (15) into equation (17), we have

$$\dot{\mathbf{B}} = 0.$$

So the boundary conditions become

$$A_{t_1} = A_{t_2} = \frac{\partial A_n}{\partial n} = 0. \tag{18}$$

The flow is assumed to be fully developed on the outlet plane. So an extrapolation technique is

used to remove the need to specify the velocity on the outlet. This is stated as

$$\frac{\partial^2 \mathbf{A}}{\partial n^2} = 0. \tag{19}$$

If the inlet plane is of the type $z = \text{const.}$ in a Cartesian system, equation (17) reduces to

$$\begin{aligned} B_x &= B_y = 0, \\ -\left(\frac{\partial^2 B_2}{\partial x^2} + \frac{\partial^2 B_2}{\partial y^2}\right) &= V_z - v_i. \end{aligned} \tag{20}$$

The boundary conditions on **A**, equation (5), become

$$\begin{aligned} A_x &= (\nabla_s \times \mathbf{B}) = \frac{\partial B_z}{\partial y}, \\ A_y &= (\nabla_s \times \mathbf{B}) = -\frac{\partial B_z}{\partial x}, \\ \frac{\partial A_z}{\partial z} &= 0 \end{aligned} \tag{21}$$

on the inlet plane.

Boundary conditions on **W**

Taking the curl of the Navier–Stokes equation yields the vorticity transport equation

$$(\mathbf{V}\cdot\nabla)\mathbf{W} - (\mathbf{W}\cdot\nabla)\mathbf{V} = \nabla^2 \mathbf{W}/Re, \tag{22}$$

where Re is the Reynolds number. The boundary conditions on **W** are relatively simple:

$$\begin{aligned} \mathbf{W} &= \nabla \times \mathbf{V} \qquad \text{on the inlet plane and walls,} \\ \frac{\partial^2 \mathbf{W}}{\partial n^2} &= 0 \qquad \text{on the outlet plane.} \end{aligned} \tag{23}$$

SOLUTION PROCEDURE

To facilitate the treatment of the boundary condition for flows in a general curved duct, the Cartesian coordinate system is transformed to a body-fitted curvilinear coordinate system. The transformed governing equations are fully described in Reference 5.

The discretization is carried out using centred differences inside the domain for all of the equations. The boundary conditions on ϕ are treated implicitly, while others are treated explicitly. In the explicit treatment, the one-sided difference formula

$$\left.\frac{\partial f}{\partial n}\right|_b = -3f_b + 4f_{b-1} - f_{b-2} \tag{24}$$

is used at the boundary nodes to ensure that the entire discretized system is of second order accuracy. Subscript b denotes the boundary point in the formula.

All the equations are solved by the block SOR method, in which the implicit block contains the nodes in one mesh line in a cross-stream direction. The relaxation parameter ω is about 1·5 for both

the scalar and the vector potential equations, while the vorticity transport equation is underrelaxed with a value of ω less than 0·7.

The overall solution procedure consists of the following steps.

(i). Generation of the body-fitted grid, and calculations of the coordinate transformation coefficients.

(ii). Computation of the scalar potential from equation (11) to the desired accuracy.

(iii). Cycling the iterative computations between the vorticity transport equation, equation (22), and the relation between **A** and **W**, equation (3), until a converged velocity field is obtained.

The iterative procedure for the scalar potential is initialized by using a linear interpolation technique. After the scalar potential is obtained to a given accuracy, the velocity field is set to the potential solution $-\nabla\phi$, The initial values of **A** and **W** are set to zero.

NUMERICAL TESTS

To evaluate the proposed numerical model, the overall algorithm was coded and several tests were carried out to help establish its accuracy, stability and efficiency.

The first test is the simulation of the development of the flow in a square duct of aspect ratio 1:1:8. Under the present set of boundary conditions, the potential velocity field is identical to a uniform vector field, so the calculation of ϕ is not necessary in this case. A viscous velocity field is computed at $Re = 50$ on a uniform grid of $11 \times 11 \times 21$. The results obtained are very similar to those calculated by Wong and Reizes.[3] This is expected since the present model is identical with theirs for this simple flow problem, except for some minor differences in the boundary conditions on **W**.

Flow in a square elbow was then simulated to evaluate the applicability of the model to curved ducts. The configuration of the elbow is shown in Figure 2. A uniform 11×11 grid was used in each cross section and 21 sections were employed along the elbow. The lengths of upstream and downstream tangents are set to be $0{\cdot}35H$ and $0{\cdot}53H$ respectively, where H is the width of the elbow.

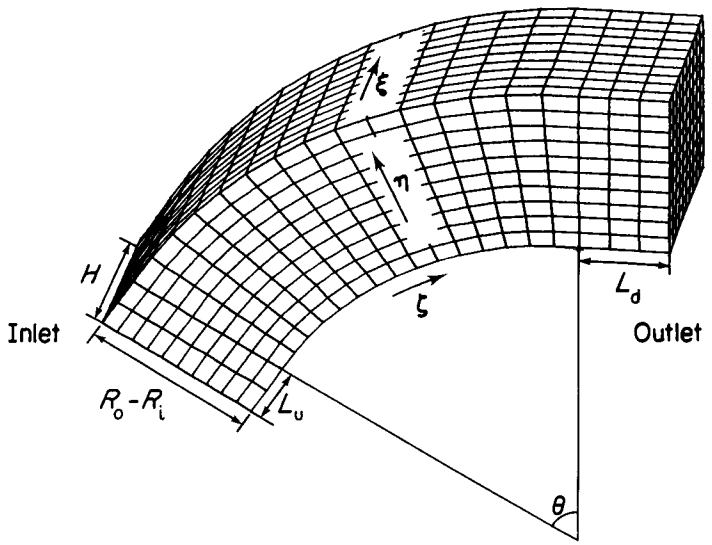

Figure 2. Description of the square elbow: $R = 2{\cdot}0$, $R = 3{\cdot}0$, $L = 0{\cdot}35$, $L = 0{\cdot}52$, $H = 1{\cdot}0$, $\theta = 60°$

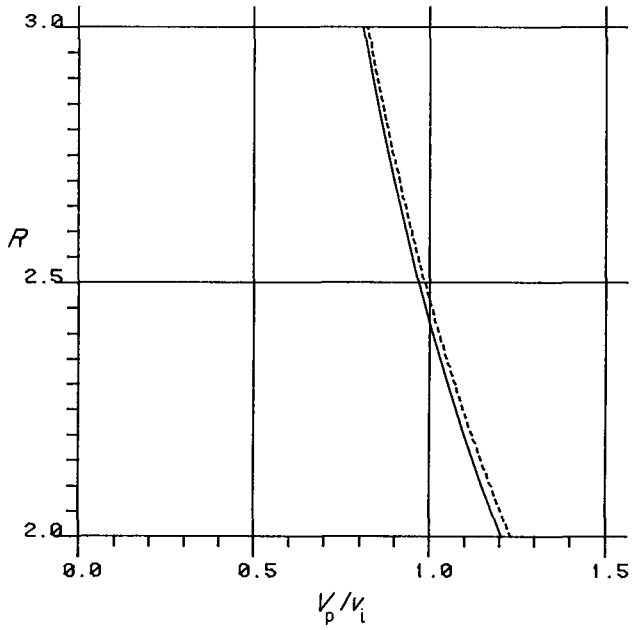

Figure 3. Streamwise profile of the potential velocity in the square elbow, Location of $\theta = 32°$:——present results; ------ analytical results

The velocities at inlet are assumed to be

$$\begin{aligned} V_z &= 36{\cdot}0xy(1-x)(1-y), \quad 0 \leqslant x \leqslant 1, \quad 0 \leqslant y \leqslant 1, \\ V_x &= 0, \\ V_y &= 0, \end{aligned} \tag{25}$$

which are similar to the velocities of fully developed flow in a square duct.

A satisfactory potential solution for this geometry required 300 iterations and about 10 min of CPU time on an IBM 4341. The R.M.S. of the residual in the converged solution is of the order of 10^{-3}. The streamwise profile of the potential velocity $-\nabla\phi$ at the section of $\theta = 32°$ (θ is the angle of turning) is compared in Figure 3 with the analytical solution of irrotational motion. It illustrates the accuracy of the potential solution and proves that the present boundary conditions on ϕ are suitable.

To add the viscous influence (with $Re = 80$), 60 cycles of computations between the vorticity transport equation, equation (22), and the relation between **A** and **W**, equation (3), were performed. The run time is about 22 min.

An interesting physical characteristic of flow in a curved duct is the development of secondary flows. Figure 4 shows that this phenomenon is reasonably simulated by the present model. The helical motion originates at the section of $\theta = 8°$, and becomes stronger as the flow turns through the duct. At the exit, the secondary flow does not disappear entirely, because the downstream tangent is relatively short, and it would require a length of $0{\cdot}07Re = 5{\cdot}6$ for the re-development of the flow. It can also be observed that, as the flow progresses, the centres of the streamwise vortices move symmetrically toward the pressure surface, drawn by the strong radial flow in the central plane. At the same time the high streamwise velocities existing near the duct centre move towards the pressure surface as indicated in Figure 5. In Figure 6 the streamwise velocity profile at

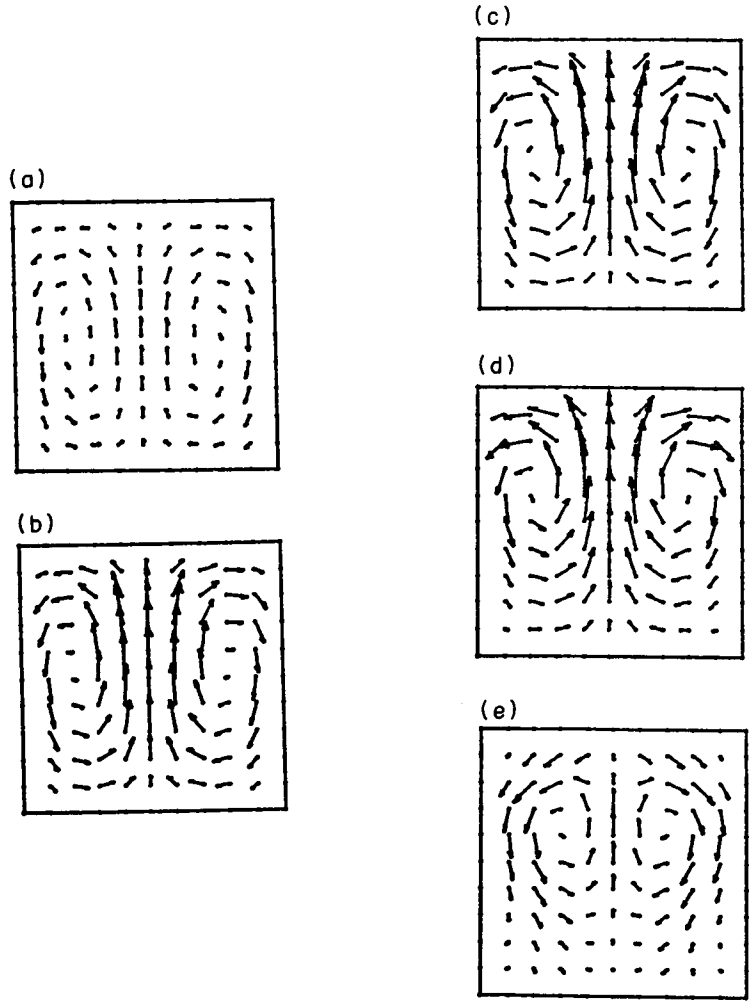

Figure 4. Development of secondary flow in the square elbow at $Re = 80$: (a) on the section of $\theta = 8°$; (b) on the section of $\theta = 24°$; (c) on the section of $\theta = 40°$; (d) on the section of $\theta = 56°$; (e) on the outlet plane

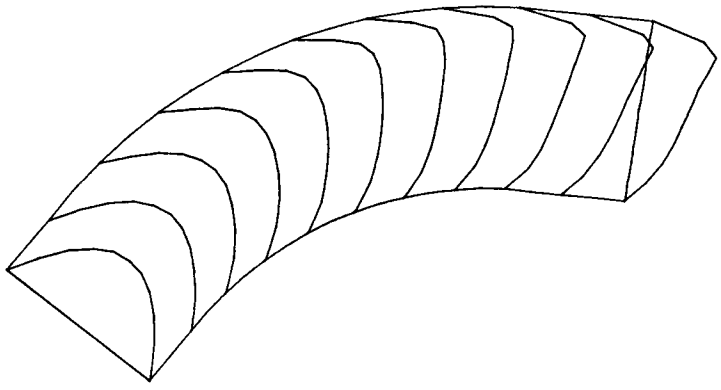

Figure 5. Development of the streamwise velocity profiles in the square elbow at $Re = 80$

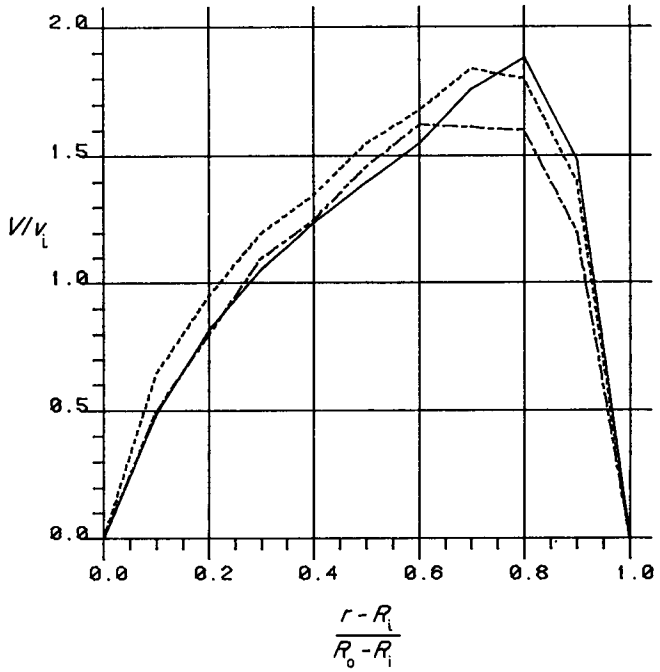

Figure 6. Fully developed streamwise velocity profile in the square elbow:——present results;----Khalil computed results;–·–·–·–·Mori measured results

the section of $\theta = 60°$ is compared with other fully developed velocity profiles: one is computed by Khalil and Weber[6] from the time averaged Navier–Stokes equations, and the other measured experimentally by Mori *et al.*[7] Near the suction surface, the present results are much closer to the measurements than those of Khalil and Weber. The two computations show almost no difference near the pressure surface. The difference between the measurements and various computations in the high velocity part has not been adequately explained yet.

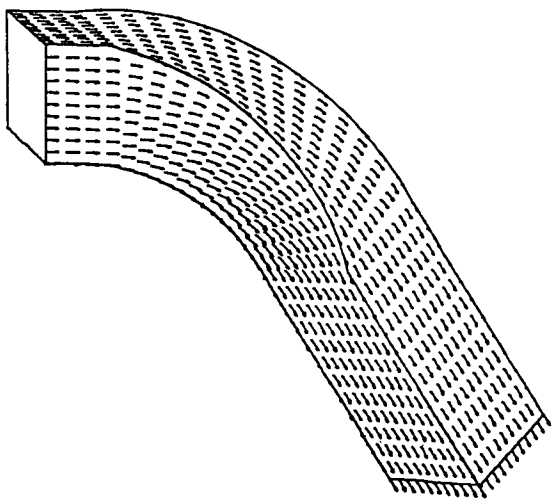

Figure 7. Potential velocity distribution on the walls of twisted elbow

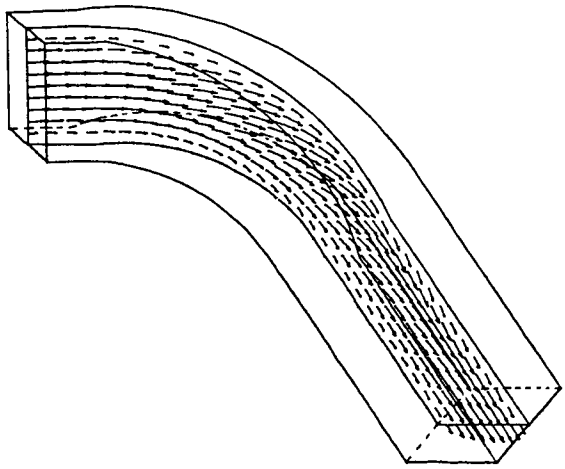

Figure 8. Central slice of velocity vector field at $Re = 80$

For the purpose of investigating the response of the present model to differences in Reynolds numbers, solutions at $Re = 10$ and 100 were also computed. From a numerical aspect, it is found that, the higher Re is, the smaller is the value of the relaxation parameter required for the vorticity transport equation. The optimal relaxation parameters used in the present series of tests are 0·7, 0·3 and 0·15 for $Re = 10$, 80 and 100, respectively. Consequently, a slower convergence is obtained for higher Reynolds numbers. For $Re = 150$, divergence resulted. To stabilize the numerical iterations for higher Re, the upwind-difference technique should be employed, as noted by Aregbesola and Burley.[4]

Another numerical test is devoted to show the capability of the present model to predict flows in complex duct. The geometry is a 60-degree turning elbow with 60-degree twist around its central line. The potential solution, shown in Figure 7, shows again that the boundary conditions on ϕ are well applied. Figure 8 presents the middle slice of the viscous velocity field at $Re = 80$. It can be clearly seen that the flow re-develops into a straight duct flow type in the downstream tangent. The velocity profile obtained at the exit is about the same as that of fully developed straight duct flow, which shows that the extrapolation technique used in the present model is acceptable in the simulation of duct flow.

ACKNOWLEDGEMENTS

This research was carried out under the PRAI grant P–8122 from NSERC of Canada and a scholarship from the government of China.

NOMENCLATURE

A	vector potential function
n	unit vector normal to boundaries
t	unit vector tangent to boundaries
V	velocity vector variable
W	vorticity vector variable
x, y, z	Cartesian coordinates
ϕ	scalar potential function

REFERENCES

1. G. J. Hirasaki and J. D. Hellums, 'A general formulation of the boundary conditions on the vector potential in three-dimensional hydrodynamics', *Quarterly of Applied Mathematics* **26**, 331–342 (1968).
2. G. J. Hirasaki and J. D. Hellums, 'Boundary conditions on the vector and scalar potentials in viscous three-dimensional hydrodynamics', *Quarterly of Applied Mathematics* **28**, 293–296 (1970).
3. A. K. Wong and J. A. Reizes, 'An effective vorticity–vector potential formulation for the numerical solution of three-dimensional duct flow problem', *Journal of Computational Physics* **55**, 98–114 (1984).
4. Y. A. S. Aregbesola and D. M. Burley, 'The vector and scalar potential method for the numerical solution of two- and three-dimensional Navier–Stokes equations', *Journal of Computational Physics* **24**, 398–415 (1977).
5. H. Yang, 'Numerical modeling of three-dimensional viscous incompressible steady-state duct flow using body-fitted coordinates system', *M.Sc.A. Thesis*, Ecole Polytechnique de Montreal, Canada, 1984.
6. I. M. Khanlil and H. G. Weber, 'Modelling of three-dimensional flow in turning channels', *ASME J. of Eng. for Turbines and Power* **106**, 682–691 (1984).
7. Y. Mori, Y. Uchida and T. Ukon, 'Forced convective heat transfer in a curved channel with a square cross section', *Int. J. Heat and Mass Transfer* **14**, 1787 (1971).